

Spectral Statistics in Chaotic Systems with Two Identical, Connected Cells

T. Dittrich[†], H. Schanz

Max-Planck-Institut für Physik komplexer Systeme, Nöthnitzer Straße 38, D-01187
Dresden, Germany

G. Koboldt[§]

Institut für Physik, Universität Augsburg, Memminger Straße 6, D-86135 Augsburg,
Germany

Abstract. Chaotic systems that decompose into two cells connected only by a narrow channel exhibit characteristic deviations of their quantum spectral statistics from the canonical random-matrix ensembles. The equilibration between the cells introduces an additional classical time scale that is manifest also in the spectral form factor. If the two cells are related by a spatial symmetry, the spectrum shows doublets, reflected in the form factor as a positive peak around the Heisenberg time. We combine a semiclassical analysis with an independent random-matrix approach to the doublet splittings to obtain the form factor on all time (energy) scales. Its only free parameter is the characteristic time of exchange between the cells in units of the Heisenberg time.

PACS numbers: 05.45.+b, 03.65.-w, 73.20.Dx

Short title: Chaotic Systems with Two Identical Cells

December 2, 2024

[†] Permanent address: Depto. de Física, Universidad de los Andes, A. A. 4976, Santafé de Bogotá, Colombia

[§] Present address: Fachbereich 7 – Physik, Universität GHS Essen, D-45117 Essen, Germany

1. Introduction

Most of the pioneering enquiries into quantum chaos have been focussed on bounded systems—closed billiards, atomic systems—whose classical dynamics knows only a single global time scale, the inverse Kolmogorov entropy which describes the ergodic coverage of phase space. The absence of other classical times has facilitated the understanding of quantum-to-classical relationships and has opened the view for universal features in spectra and eigenfunctions of classically chaotic systems.

Extended systems represent another, still simple, extreme. They reach ergodicity only on a time scale that exceeds all other characteristic times. With extended systems, basic solid-state concepts enter quantum chaos. The crucial rôle of long-range spatial order, in particular, for spectrum and transport has to be considered in the unfamiliar context of dynamical disorder. In a semiclassical approach, some light could recently be shed on the spectral signatures of chaotic diffusion, both in the band structure of periodic systems [1] and in the discrete spectra of disordered systems with localized eigenstates [2, 3, 4].

A region intermediate between bound and extended is marked by systems comprising just a few similar cells. In the following, we will consider spatial confinements or phase-space structures that decompose into two compartments, connected only by a “bottleneck” (Fig. 1) [5]. Equilibration between the cells then takes much longer than the ergodic coverage of a single cell. It constitutes a second independent time scale of the classical dynamics.

Chaotic systems with two cells have quite diverse applications. They can serve as models for non-ergodic reaction dynamics in quantum chemistry [6]. More generally, they form prototypes of systems decomposing into two similar, weakly coupled parts. In this sense, they can represent heavy nuclei in a final state of fission [7], or nuclei with their two isospin subsystems interacting weakly due to a slight breaking of isospin invariance [8].

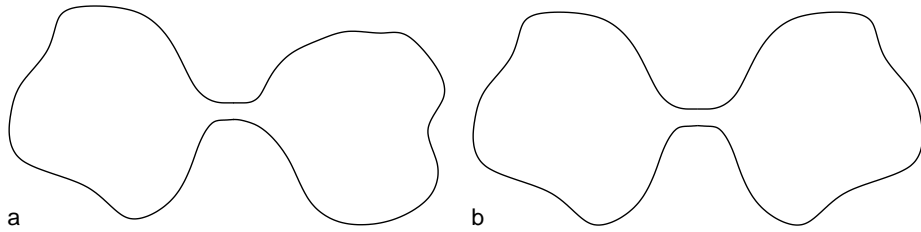


Figure 1. Two-cell billiard with narrow bottleneck, of arbitrary (a) and reflection-symmetric shape (b).

In their quantum-mechanical properties, two-cell systems already exhibit the decisive influence of spatial symmetry. If the two cells are of arbitrary shape or size

(Fig. 1a), their restricted communication will be reflected in a quantitative deviation from the canonical random-matrix statistics [5]. It does not introduce any qualitatively new feature. The situation changes considerably if the cells are related by some twofold unitary symmetry (Fig. 1b). A genuine quantum phenomenon, a coherent mode of transport between the cells emerges, and the spectrum shows systematic quasidegeneracies. This clustering of levels is manifest in the two-point correlations as a marked *positive* peak on the scale of the mean single-cell level separation, or in the time domain, the single-cell Heisenberg time [1].

This phenomenon should be carefully distinguished from tunneling. To be sure, the doublets do resemble tunnel splittings in that they are based on a discrete spatial symmetry and correspond to quantum coherent transport on very long time scales. Moreover, in the wavenumber regime where there is no open channel in the constriction between the cells, the wavefunctions decay exponentially into this region. Even at higher wavenumber, the amplitude is often strongly suppressed there (cf. Fig. 9). Since, however, there is neither a potential nor a dynamical barrier involved, this transport is slow but not classically forbidden.

Chaos-assisted tunneling is a hallmark of bistable systems with a mixed phase space [9, 10, 11]. It occurs between symmetry-related pairs of *regular* islands in phase space that are separated by a chaotic region. Here, by contrast, we are dealing with symmetry-related *chaotic* regions communicating through a narrow bridge in space. Still, a similar situation can occur also in mixed bistable systems. In fact, the distribution of the splittings of doublet states supported by symmetry-related pairs of chaotic regions forms an important input to the distribution of tunnel splittings in chaos-assisted tunneling [12].

In the following sections, we shall develop a theory for the spectral statistics of two-cell systems that largely rests on recent progress in the analysis of band structures of classically chaotic systems with spatial periodicity [1]. There, an important input has been the notion of form factors with a winding-number argument, specific for transitions spanning a corresponding number of unit cells. Likewise, the group property of a reflection or translation symmetry of a two-cell system enables the definition of form factors with a rudimentary spatial resolution, expressed by a binary index that indicates either return to the same cell or transitions into the opposite cell.

However, as compared to [1], we do not only go from a large value of N , the number of unit cells, to $N = 2$. Here, we shall concentrate on the case of slow exchange between the cells, the “weak-coupling” or “tight-binding” limit in solid-state terminology, while [1] was devoted to the opposite case. This implies that, even if the two-cell system is “unfolded” to form an infinite chain, the concept of homogeneous diffusion no longer applies. Rather, in the unfolded picture, we are dealing with a spatially discrete diffusion process that deviates significantly, on short time scales, from ordinary diffusion.

Concerning the spectral statistics, the principal consequence is that we are now dealing with flat “bands”.

In order to extend a semiclassical treatment of the spectral correlations to energy scales below the mean level spacing, information on the spreading of the possibly complex trajectories that mediate the long-time transitions [13, 14], analogous to the sum rules for ergodicity [15] or diffusion [2, 3], would be required. Alternatively, we would have to surmount the diagonal approximation. We circumvent this open problem and instead adopt a different strategy. In the spirit of Berry’s semiclassical approximation for the form factors of random-matrix ensembles [16], we impose plausible assumptions on the distribution of the narrow splittings. They are based on the relation of the doublet splittings in two-cell compounds to the resonance widths in corresponding single-cell systems, obtained by opening up the system at the constriction. We derive this relation in the case of a single open channel between the cells, where it deviates from the identity.

Switching back from the distribution of doublet splittings to the corresponding time-domain function valid on long time scales, we match this long-time asymptote with the semiclassical short-time behaviour. In this way, we achieve expressions for the spectral two-point correlations on all time scales. They are universal in that they contain, as the only free parameter, the characteristic time for equilibration between the cells. It is the two-cell analogue of the conductance, the scaling parameter in the case of long chains.

We shall introduce the classical concepts relevant for the dynamics of systems with two identical, connected cells in the subsequent Section 2. In Section 3, we define form factors specific for an element of the symmetry group of the system. A semiclassical theory for the short-time regime of these form factors is developed in Section 4, while Section 5 is devoted to their quantum long-time behaviour. Some of these calculations are extended to the case of general N in two appendices. Section 6 serves to introduce four illustrative models, two versions of a Sinai billiard [1, 17], quantum graphs [18] configured in such a way that they form a two-cell system, and a two-cell variant of the quantum kicked rotor [19, 1]. Spectral data obtained numerically for these models corroborate our theory. Section 7 contains a synopsis of the various limiting cases covered in this paper.

2. Classical dynamics in two-cell systems

As a minimal version of a classical two-cell system, consider the following model: Two spatially confined compartments of arbitrary shape, size, and internal structure are connected by some narrow duct (Fig. 1a). In view of the intended applications, we require a few additional properties. The leakage from the cell where the system is prepared (subscript ‘0’ in the following) to the opposite side (subscript ‘1’) should be

completely described by a single time scale $1/\lambda$. This amounts to an exponential decay of the population from the cells, if they were opened by removing the opposite cell. We require the rate λ to be the same in both directions, a sufficient condition for which is that the cells form a (translation- or reflection-) symmetric pair (Fig. 1b). Finally, we assume that the dynamics within the cells is chaotic and thus ergodic, and that coverage of a single cell is reached instantaneously on the scale $1/\lambda$.

Under these conditions, the time evolution of the probability to stay in either cell obeys the simple pair of master equations,

$$\begin{aligned}\dot{P}_0(t) &= \lambda (P_1(t) - P_0(t)), \\ \dot{P}_1(t) &= \lambda (P_0(t) - P_1(t)).\end{aligned}\tag{1}$$

The relaxation into equilibrium of the two probabilities, given by $\lim_{t \rightarrow \infty} P_{0/1}(t)/(P_0(t) + P_1(t)) = 1/2$, is governed by the rate $\Lambda = 2\lambda$. From an initial state $P_0(0) = 1$, $P_1(0) = 0$, they evolve as

$$P_{0/1}(t) = \frac{1}{2}(1 \pm e^{-\Lambda t}).\tag{2}$$

The population difference

$$P_d(t) = P_0(t) - P_1(t)\tag{3}$$

is another relevant quantity. Besides the sum $P_0(t) + P_1(t)$, it plays the rôle of an eigenmode amplitude of the master equation (1). Its time evolution reads, for the same initial state as above,

$$P_d(t) = e^{-\Lambda t}.\tag{4}$$

The above considerations apply also if the cells communicate through two or more physical channels. This includes in particular the case of two cells connected at both “ends” to form a ring. The rates of probability exchange through the channels then just add to give the global rate λ . The diffusive dynamics that results if a two-cell ring configuration is unrolled into an infinite chain, is discussed in Appendix A.

3. Generalized form factors

In quantum systems, each unitary symmetry gives rise to a constant of the motion, a “good quantum number”. It takes as many values as there are irreducible representations of the symmetry, and the full spectrum can be decomposed into subspectra, each of which pertains to a given representation. Formally, the decomposition is effected by the projectors [20] $\hat{P}_m = N^{-1} \sum_{n=0}^{N-1} \chi_m(g_n) \hat{U}^\dagger(g_n)$, $m = 0, \dots, N-1$. Here, N is the number of elements g_n of the symmetry group and simultaneously the number of its representations (for simplicity, we assume all

representations to be one dimensional). The character of g_n in the m th representation is referred to as $\chi_m(g_n)$, and $\widehat{U}(g_n)$ denotes the unitary transformation corresponding to g_n . Spectral densities and correlation functions within a given representation can then be defined on basis of the symmetry-projected Green function $\widehat{G}_m(E) = \widehat{P}_m \widehat{G}(E)$, with $\widehat{G}(E)$, the Green function for the entire spectrum. For example, the symmetry-projected spectral density in the m th representation is defined as

$$d_m(E) = \sum_{\alpha} \delta(E - E_{\alpha,m}) = -\frac{1}{\pi} \text{Im} \text{tr} [\widehat{G}_m(E)], \quad (5)$$

where the $E_{\alpha,m}$ are the eigenenergies in the m th representation.

For the study of quasidegenerate doublets, another type of spectral density is as relevant as the symmetry-projected one. Alternatively, one may define densities and derived quantities that refer to a group element g_n , instead of an irreducible representation m . The symmetry group induces a decomposition of the (phase) space at hand into disjunct segments, such that each of them is mapped onto all the others by the transformations in the group, thus covering the entire space [21]. A group-element-specific spectral density therefore provides a rudimentary spatial resolution on the scale of the tessellation of space by the group.

If all representations are one dimensional, the set of columns of the matrix $\chi_{m,n} = \chi_m(g_n)$ of group characters forms an orthogonal basis in N dimensions [20]. The same is true for the rows. The matrix as a whole therefore has full rank and is invertible. We refer to the inverse matrix as χ^{-1} . Multiplying the vector of symmetry-reduced spectral densities $d_m(E)$, Eq. (5), from the left by χ^{-1} , we obtain the spectral densities [1]

$$\tilde{d}_n(E) = \sum_{m=0}^{N-1} (\chi^{-1})_{m,n} d_m(E) \quad (6)$$

$$= -\frac{1}{\pi} \text{Im} \int_{\text{fd}} \text{d}q \widehat{G}(g_n(\mathbf{q}), \mathbf{q}; E). \quad (7)$$

The space integral in Eq. (7) extends only over the fundamental domain (subscript ‘fd’) of the tessellated space. The first argument of the Green function in the third line is the image of its second argument, \mathbf{q} , under g_n . This suggests that $\tilde{d}_n(E)$ refers to transitions from any segment to its image under g_n .

By Fourier transforming Eq. (6) with respect to energy, we arrive at the analogous density in the time domain,

$$\tilde{a}_n(\tau) = \langle d_{\text{fd}} \rangle^{-1} \int_{-\infty}^{\infty} \text{d}r e^{-2\pi i r \tau} \tilde{d}_n(r / \langle d_{\text{fd}} \rangle) \quad (8)$$

$$= \int_{\text{fd}} \text{d}q \langle g_n(\mathbf{q}) | \widehat{U}(t_{\text{H}} \tau) | \mathbf{q} \rangle. \quad (9)$$

We have switched to dimensionless energy, $r = \langle d_{\text{fd}} \rangle E$, and time, $\tau = t/t_{\text{H}}$, by scaling with the mean spectral density $\langle d_{\text{fd}} \rangle$ in the symmetry-reduced space, and the

corresponding Heisenberg time $t_H = 2\pi\hbar\langle d_{\text{fd}} \rangle$, respectively. Equation (9) describes an amplitude to return modulo the symmetry transformation g_n . The corresponding return probability is given by the form factor

$$\tilde{K}_n(\tau) = \frac{1}{\Delta r_{\text{fd}}} |\tilde{a}_n(\tau)|^2, \quad (10)$$

where Δr_{fd} is the total width, in units of $\langle d_{\text{rs}} \rangle$, of the spectrum considered.

For a two-cell system, a symmetry that maps one cell to the other can be a reflection or a translation. Their group elements are identity (denoted by $n = 0$ in the following) and reflection or translation ($n = 1$, without distinguishing the two). The characters are both 1 in the symmetric (subscript '+') representation, and ± 1 in the antisymmetric ('-') representation. Following the general discussion above, we define symmetric and antisymmetric form factors, respectively, by

$$K_{\pm}(\tau) = \frac{1}{\Delta r_{\text{fd}}} |a_{\pm}(\tau)|^2. \quad (11)$$

The amplitudes $a_{\pm}(\tau)$ are obtained, for example, by sorting the spectral data according to the symmetry of the corresponding eigenstates, and Fourier transforming as in Eq. (8). Form factors specific for return to the initial (subscript '0') or switching to the opposite cell ('1') are defined according to Eq. (6) and Eqs. (8), (10) as

$$\tilde{K}_{0/1}(\tau) = \frac{1}{\Delta r_{\text{fd}}} |a_+(\tau) \pm a_-(\tau)|^2. \quad (12)$$

By comparing Eqs. (11) and (12), we see that the sums of the symmetry-projected and the group-element-specific form factors are the same,

$$\tilde{K}_0(\tau) + \tilde{K}_1(\tau) = K_+(\tau) + K_-(\tau). \quad (13)$$

This identity may be interpreted as a preservation of norm and follows generally from the unitarity of the matrix $\chi_{m,n}$ of group characters.

In the following, when dealing with two-cell systems, we shall drop the tilde and distinguish the various form factors only by their subscripts. Note that in Eq. (12), amplitudes are superposed *before* squaring. We shall show in Sect. 5 below that considering the *incoherent* superpositions $K_0(\tau) \pm K_1(\tau)$, in turn, provides an approximate access to the distribution of doublet splittings and inter-doublet separations, respectively.

4. Semiclassical regime

In order to construct a semiclassical trace formula for the symmetry-projected spectral density $d_m(E)$, Eq. (5), the concept of periodic orbits has to be extended [21]. In case the dynamics within the cells has no significant admixture of regular motion, the trace

formula reads

$$d_m^{(\text{sc})}(E) = \frac{D_m}{i\hbar N} \sum_j \frac{T_j^{(\text{p})}}{\kappa_j \sqrt{|\det(M_j - I)|}} \times \chi_m(g_j) \exp\left(i\frac{S_j}{\hbar} - i\mu_j \frac{\pi}{2}\right) \quad (14)$$

The sum now runs over generalized period orbits j . Their end point is not necessarily identical with the starting point, but must be mapped to it by some group element g_j . The corresponding term in Eq. (14) then contains the character $\chi_m(g_j)$ as an extra, non-classical phase factor. A correction of the amplitude for orbits that coincide with symmetry lines is effected by κ_j [21]. As usual, $T_j^{(\text{p})}$, M_j , S_j , μ_j denote primitive period, stability matrix, classical action, and Maslov index, respectively, of orbit j .

The rôle of the generalized periodic orbits becomes even more transparent in the analogous trace formula for the group-element-specific density,

$$\tilde{d}_n^{(\text{sc})}(E) = \frac{1}{i\hbar N} \sum_j \frac{T_j^{(\text{p})}}{\kappa_j \sqrt{|\det(M_j - I)|}} \times \delta(g_j, g_n) \exp\left(i\frac{S_j}{\hbar} - i\mu_j \frac{\pi}{2}\right). \quad (15)$$

The delta function in the second line equals unity if its arguments coincide and vanishes otherwise. It selects orbits j whose endpoints are connected by g_n . They mediate transport from the original segment to its image, with the restriction that initial and final points are exactly related by the symmetry.

The interpretation that spectral quantities associated with g_n describe transport from an original space segment to its image under g_n is borne out quite explicitly by the form factors. A semiclassical expression for the $\tilde{K}_n(\tau)$ can be derived by substituting the trace formula (15), Fourier transformed to the time domain as in Eq. (8), into Eq. (10). Within the diagonal approximation with respect to pairs of generalized periodic orbits [16, 1, 2, 3, 4], which is valid for times $t \ll t_{\text{H}}$, one obtains,

$$\tilde{K}_n^{(\text{sc})}(\tau) = \gamma_n \tau P^{(\text{cl})}(g_n, \tau t_{\text{H}}), \quad \tau \ll 1. \quad (16)$$

Equation (16) relates the form factors to the classical probability $P^{(\text{cl})}(g_n, t)$ to return in time t to a phase-space point related to the starting point by g_n . The contribution of repetitions of shorter periodic orbits has been neglected in Eq. (16). By introducing a global degeneracy factor γ_n to account for anti-unitary symmetries like time-reversal invariance, we ignored the occurrence of self-retracing orbits. This factor takes the value 2 if orbits that are periodic modulo g_n are generically time-reversal degenerate, and 1 else. A non-trivial dependence of γ_n on n can occur, e.g., in periodic systems with $N \geq 3$ unit cells [1]. There, time-reversal invariance is generally broken for orbits with winding numbers $n \bmod N \neq 0, N/2$, due to Bloch phases that are not real.

In the spirit of the known classical sum rules for ergodic systems [15], we assume that the generalized periodic orbits are not distinct from the generic non-periodic ones in their average spreading. We can then relate the $P^{(\text{cl})}(g_n, t)$ to the classical propagator $p(\mathbf{r}', \mathbf{r}; t)$ by a phase-space integration over the fundamental domain,

$$P^{(\text{cl})}(g_n, t) = \int_{\text{fd}} d\mathbf{r} p(g_n(\mathbf{r}), \mathbf{r}; t), \quad (17)$$

where $\mathbf{r} = (\mathbf{p}, \mathbf{q})$ denotes a phase-space point within the unit cell on the energy shell. In case that $p(g_n(\mathbf{r}), \mathbf{r}; t)$ depends on g_n but not on \mathbf{r} , the integration in Eq. (17) becomes trivial and results in

$$P_n^{(\text{cl})}(t) = \omega_{\text{fd}} p(g_n; t), \quad (18)$$

with $\omega_{\text{fd}} = d\Omega_{\text{fd}}(E)/dE$ denoting the energy-shell volume of the reduced space.

For the group-element-specific form factors defined for two-cell systems, Eq. (12), the semiclassical expression reads

$$K_{0/1}^{(\text{sc})}(\tau) = \gamma \tau P_{0/1}^{(\text{cl})}(\tau t_{\text{H}}). \quad (19)$$

Here, $P_0^{(\text{cl})}(t)$ denotes the probability to literally return to the initial phase-space point, while $P_1^{(\text{cl})}(t)$ refers to returning to the symmetry-related point in the opposite cell. We have used that in symmetric two-cell systems, the degeneracy factor γ does not depend on g_n .

In order to evaluate Eq. (19) further, explicit expressions for $P_{0/1}^{(\text{cl})}(t)$ have to be inserted. It is tempting to identify them with the total probabilities $P_{0/1}(t)$, Eq. (2), for being in the original or the opposite cell, respectively. This is equivalent to using Eq. (18) instead of the more general Eq. (17). It requires that the chaotic coverage of the single cells is homogeneous. A detailed investigation of this question for a double billiard, see Sect. 6 below, shows that there can be deviations from this condition. In that case, however, where they are due to a collimation of trajectories by the connecting duct, their effect is indeed negligible.

Within the approximation Eq. (18), we have

$$K_{0/1}^{(\text{sc})}(\tau) = \frac{\gamma \tau}{2} (1 \pm e^{-2\lambda t_{\text{H}} \tau}), \quad \tau \ll 1. \quad (20)$$

Equation (20) explicitly shows the significance of the second time scale, $1/\lambda$, besides the Heisenberg time. For $\lambda t_{\text{H}} \gg 1$, corresponding to a wide open duct, equilibration between the cells occurs instantaneously, the two form factors become indistinguishable and approach the short-time behaviour of the Gaussian unitary or orthogonal random-matrix ensembles (GUE, GOE), for $\gamma = 1$ or 2 , respectively, that is, $K_0(\tau) = K_1(\tau) = K_{\text{RMT}}(\tau)$. This is the limit of simple ergodic systems. The opposite limit of $\lambda t_{\text{H}} \ll 1$ corresponds to nearly uncoupled cells. The spectrum then consists exclusively of quasidegenerate doublets. The form factor $K_0(\tau)$, which is equivalent to the ordinary form factor up

to normalization, is then related to the corresponding canonical random-matrix form factor by a scaling of time, $K_0(\tau) = K_{\text{RMT}}(2\tau)$ [22]. In the same limit, $K_1(\tau)$ vanishes in the semiclassical time regime.

5. Long-time regime

In the semiclassical time range, we succeeded to express the form factors for all parameter regimes, from two-cell systems without significant separation of the cells to pairs of nearly uncoupled cells, by a single expression, Eq. (20). We cannot achieve this generality for the regime of long times $t \gtrsim t_H$. The case of weakly coupled ($\lambda t_H \ll 1$) symmetric billiards, to be considered here, requires additional input besides the classical information contained in Eq. (20). At the same time, this is the most interesting situation because only here, quasidegenerate doublets occur with a splitting much smaller than their typical separation.

As a starting point for an alternative approach valid in the long-time regime, we return to the exact definition of the group-element-specific amplitudes $a_{0/1}(\tau)$. Specializing Eq. (8) to the two-cell case and inserting the definition (5) of $d_{0/1}(E)$, we obtain

$$a_n(\tau) = \frac{1}{2} \sum_{m=0}^1 e^{\pi i n m} \sum_{\alpha=1}^{N_d} e^{-2\pi i \tau r_{\alpha,m}}, \quad n = 0, 1. \quad (21)$$

Here, N_d is the number of doublets in the spectrum, i.e., half the total number of levels. We have used the fact that the inverse characters for the twofold reflection or translation group can be concisely written as $(\chi^{-1})_{m,n} = e^{\pi i n m}$, with $m = 0, 1$ corresponding to the symmetric and the antisymmetric representations, respectively. In these representations, returning to the symbols ‘+’ and ‘-’, $r_{\alpha,0/1} = r_{\alpha,\pm} = \langle d_{\text{fd}} \rangle E_{\alpha,\pm}$ denote the scaled eigenenergies.

We introduce the concept of doublets by writing the eigenenergies as

$$r_{\alpha,\pm} = R_\alpha \pm r_\alpha. \quad (22)$$

The long-time limit of the form factors for the canonical random-matrix ensembles is usually derived under the assumption that the full phases τr are random for $\tau \gg 1$. Likewise, we here assume the analogous phases τR_α contributed by the doublet midpoints to be random in the long-time limit. Upon squaring the amplitudes $\tilde{a}_\pm(\tau)$ to obtain the corresponding form factors, this amounts to a diagonal approximation with respect to the index α ,

$$K_{0/1}(\tau) = \frac{1}{2} \pm \frac{1}{2N_d} \sum_{\alpha=1}^{N_d} \cos(4\pi\tau r_\alpha). \quad (23)$$

In fact, Eq. (23) can be derived also if the two-cell system is unrolled to an infinite chain and the doublets are considered as points of continuous bands, see Appendix B.

If N_d is sufficiently large, we can replace the sum over α by an integral and consider the integration as a Fourier transformation, to obtain

$$K_{0/1}(\tau) = \frac{1}{2} (1 \pm p_d(2\tau)), \quad (24)$$

with

$$p_d(\tau) = \int_0^\infty dr \cos(2\pi r\tau) p_d(r). \quad (25)$$

This is the Fourier transform of the distribution

$$p_d(r) = \sum_{\alpha=1}^{N_d} \delta(r - |r_{\alpha,-} - r_{\alpha,+}|) \quad (26)$$

of doublet splittings.

Forming the difference of the two form factors,

$$p_d(\tau) = K_0(\tau/2) - K_1(\tau/2), \quad (27)$$

we see that this equals the time-domain splitting distribution in its long-time, or equivalently, low-energy limit. Given that the form factors contain information merely on two-point correlations, it is actually surprising that they can be related, as in Eq. (27), to a quantity that requires an unambiguous identification of doublets. This can be explained by the fact that we had to assume in the derivation that the midpoints R_α of the doublets are statistically independent of their splittings r_α , which requires a clear separation of scales between splittings and spacings of doublets. Indeed, Eq. (27) ceases to be valid for $\tau \lesssim 1$, corresponding to the regime of large r_α .

We do not have any semiclassical access to $p_d(r)$. In order to nevertheless make some progress, we shall resort to results of random-matrix theory on the distribution of resonance widths, and argue that the doublet splittings obey a similar distribution.

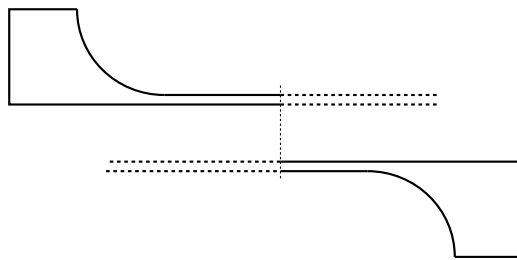


Figure 2. Two identical scattering systems are obtained when the channel connecting the two halves of a symmetric two-cell billiard is replaced by a semi-infinite waveguide of constant width. We argue that small doublet splittings between states of the two-cell billiard correspond to narrow resonances of the scattering systems (see text).

Suppose the channel between the two cells to be replaced by a semi-infinite duct of constant width, so that two single cells remain, each with a small opening that couples

its interior to the continuum in the duct. This situation is illustrated with a symmetric two-cell billiard in Fig. 2. The spectra of the open single cells will then exhibit narrow resonances at roughly the same energies where the corresponding closed two-cell system shows doublets. It is plausible that the doublet splittings of the two-cell configuration are related to the resonance widths in the single-cell setup, at least in a statistical sense. Indeed, this assumption is often made, e.g., in nuclear theory, and supported by semiclassical and random-matrix arguments. In short, it is justified by the fact that both quantities, widths and splittings, can be expressed by the same wavefunction overlaps and therefore obey the same distribution.

Here we are interested in the case of very few open channels in the connecting section, since this is required for the formation of genuine doublets. In this limit, we cannot expect random-matrix theory to remain valid. However, taking the point of view of the scattering approach to quantization [23], we show in the following paragraphs that there is still a close relation, though not an exact identity, between the respective distributions of widths and splittings.

We shall consider specifically the wavenumber regime where there is just a single open channel in the connecting section. This case is realized in the majority of the numerical examples below. Here, the calculation is particularly straightforward and transparent, because the scattering in the cell is described by a 1×1 scattering “matrix” (since there is only one opening, all incoming waves leave as reflected waves). As we are interested in isolated narrow resonances, we assume their widths to be small as compared to their separations. The S matrix can then be written in the form

$$S(r) = e^{i\theta} \frac{r - r_0 - ig}{r - r_0 + ig}, \quad (28)$$

where $r_0 - ig$ denotes the position of the resonance pole in the complex energy plane, again in units of the mean level spacing. The quantization condition in terms of $S(r)$ is [23]

$$S(r_{\pm}) = \pm 1, \quad (29)$$

the upper sign referring to the case of symmetric states (subscript ‘+’), the lower one to antisymmetric states (‘-’). Inserting Eq. (28) gives the eigenvalues

$$r_+(\theta) = r_0 + g \cot \theta/2, \quad (30)$$

$$r_-(\theta) = r_0 - g \tan \theta/2, \quad (31)$$

for the symmetric and antisymmetric cases, respectively, separated by the splitting

$$r(\theta) = |r_-(\theta) - r_+(\theta)| = \frac{2g}{|\sin \theta|}. \quad (32)$$

This function is π periodic. In the interval $0 \leq \theta < \pi$, it has a minimum at $\theta = \pi/2$, with functional value $r(\pi/2) = 2g$. It diverges at $\theta = 0, \pi$.

This analysis already exhibits the essential facts to be demonstrated: There is a connection between resonance widths and doublet splittings, but it depends on the unknown value of the total phase θ of the S matrix. As no value of θ is singled out a priori, we assume equidistribution of the total phase. Under this condition, the main contribution to the distribution of the splittings comes from $r_s \gtrsim 2g$. This is the simple relation between doublet splittings and resonance widths we seek. Quantitatively, we find the probability density

$$p_d(r|g) = \frac{4g}{\pi r^2} \left(1 - \left(\frac{2g}{r}\right)^2\right)^{-1/2} \quad (r \geq 2g). \quad (33)$$

for the splittings. It is normalized to unity, but already its first moment diverges. Indeed, as we started from the assumption of small splittings, we cannot expect the result to be valid for large splittings. The missing cutoff will be given by our semiclassical considerations which cover the complementary regime of large splittings.

The distributions of wave-function amplitudes and of resonance widths are among the established principal results of random-matrix theory [24]. Even if details of their application to quantum chaotic scattering are still under study, we can, for the present purposes, adopt the canonical random-matrix results for $p(g)$, the probability density of the resonance widths, and substitute them to obtain the unconditional splitting distribution $p_d(r)$.

Its general relation with the conditional $p_d(r|g)$ and $p(g)$ reads

$$p_d(r) = \int_0^\infty dg p(g) p_d(r|g). \quad (34)$$

In order to get back from the energy to the time domain, we perform a Fourier transformation of $p_d(r)$, cf. Eq. (25). Inserting the explicit expression (33) for $p_d(r|g)$, we obtain

$$p_d(\tau) = \frac{1}{\pi} \int_0^1 dx \frac{2}{\sqrt{1-x^2}} p\left(\frac{2\tau}{x}\right), \quad (35)$$

where $p(\tau) = \int_0^\infty dg \cos(2\pi g\tau) p(g)$, in turn, is the Fourier transform of the distribution of resonance widths.

For time-reversal-invariant systems, the resonance widths obey a Porter-Thomas distribution [24]

$$p_{PT}(g) = \frac{e^{-g/2\langle g \rangle}}{\sqrt{2\pi\langle g \rangle g}}. \quad (36)$$

The integral obtained by inserting the Fourier transform

$$p_{PT}(\tau) = \sqrt{\frac{1 + \sqrt{1 + [4\pi\langle g \rangle\tau]^2}}{2(1 + [4\pi\langle g \rangle\tau]^2)}} \quad (37)$$

into (35) can be used for a numerical computation of the form factor. In the long-time limit we find from an asymptotic expansion of (37)

$$p_d(\tau) = \frac{1}{4\pi} \frac{\Gamma(3/4)}{\Gamma(5/4)} \frac{1}{\sqrt{\langle g \rangle \tau}} + O\left((\langle g \rangle \tau)^{-3/2}\right). \quad (38)$$

If time-reversal invariance is broken, the resonance widths are exponentially distributed,

$$p_{\text{exp}}(g) = \frac{1}{\langle g \rangle} e^{-g/\langle g \rangle}, \quad (39)$$

$$p_{\text{exp}}(\tau) = \frac{1}{1 + (2\pi\langle g \rangle \tau)^2} \quad (40)$$

and accordingly

$$p_d(\tau) = \frac{1}{1 + 4\pi\langle g \rangle \tau \sqrt{1 + (4\pi\langle g \rangle \tau)^2} + (4\pi\langle g \rangle \tau)^2}. \quad (41)$$

For $\langle g \rangle \tau \gg 1$ we find $p_d(\tau) \rightarrow (4\pi\langle g \rangle \tau)^{-2}/2$.

Please note that for both, exponential and Porter-Thomas distribution, the asymptotic behaviour of the doublet splittings for large time/small energy is equivalent to the corresponding resonance-width distribution up to a constant prefactor which relates the mean doublet splitting to $\langle g \rangle$. This constant—it equals $2\pi\Gamma^2(\frac{5}{4})/\Gamma^2(\frac{3}{4}) \approx 3.44$ with and $\sqrt{8} \approx 2.82$ without time-reversal invariance—is somewhat above 2 as anticipated from Eq. (32).

In Fig. 3, we compare the Fourier-transformed unconditional splitting distribution Eq. (35) in the presence and absence of time-reversal invariance to the corresponding distribution of resonance widths for $\langle g \rangle = 0.1$. We see that for $\langle g \rangle \tau \gtrsim 1$, the deviation between the two is not dramatic and conclude that the resonance distribution $p(g)$, Porter-Thomas or exponential, is the crucial input for $p_d(\tau)$, while it is quite robust against changes and approximations entering via $p_d(r|g)$.

Now we return to our main line of reasoning and attempt a matching of the short-time (large-separation) with the long-time (small-splitting) regime of the form factors. This will simultaneously allow us to calibrate the as yet undetermined parameter $\langle g \rangle$ of the resonance distribution with respect to the classical decay rate λ . We shall present this calculation only for the simpler case of broken time-reversal invariance, the matching procedure for systems with time-reversal symmetry will be discussed in detail in subsection 6.2.

From the semiclassical side, Eq. (20), we find at the matching point $\tau = 1$,

$$K_{0/1}(1) = \frac{1}{2} \left(1 \pm e^{-2\lambda t_H} \right), \quad (42)$$

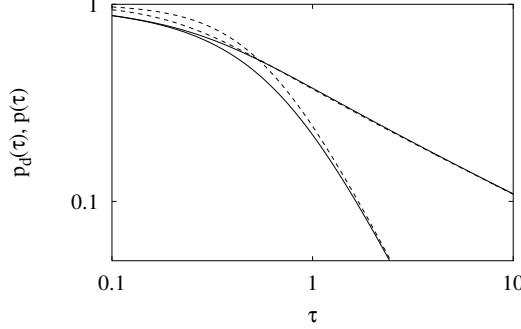


Figure 3. Time-domain splitting distribution Eq. (35) for symmetric two-cell systems with a single open channel in the connector, in the presence of time-reversal invariance (upper solid line) and in its absence (lower solid line). For comparison, the broken lines show the Fourier-transforms of the corresponding resonance distributions, i.e., of the Porter-Thomas distribution Eq. (37), above, and of the exponential distribution Eq. (40), below. The parameter value common to all curves is $\langle g \rangle = 0.1$.

while from the long-time side, substituting Eq. (41) in Eq. (24), we have

$$K_{0/1}(1) = \frac{1}{2} \left(1 \pm \frac{1}{1 + c\sqrt{1 + c^2} + c^2} \right), \quad (43)$$

introducing the shorthand $c = 8\pi\langle g \rangle$. These equations are consistent with one another if

$$e^{-2\lambda t_H} = \frac{1}{1 + c\sqrt{1 + c^2} + c^2}, \quad (44)$$

or, resolving for c ,

$$c = \frac{1 - e^{-2\lambda t_H}}{\sqrt{e^{-2\lambda t_H}(2 - e^{-2\lambda t_H})}}. \quad (45)$$

We state the full time dependence of the form factors in the long-time regime, again using the abbreviation c for the sake of conciseness,

$$K_{0/1}(\tau) = \frac{1}{2} \left(1 \pm \frac{1}{1 + c\tau\sqrt{1 + c^2\tau^2} + c^2\tau^2} \right). \quad (46)$$

In Fig. 4, we give a synopsis of $K_{0/1}(\tau)$ (a) and $Y_{0/1}(r) = \int_0^\infty d\tau [1 - K_{0/1}(\tau)] \cos(2\pi r\tau)$ (b), for values of the decay constant ranging from $\lambda \ll 1$ to $\lambda \approx 1$. The figure illustrates the crossover of the spectral two-point correlations from the regime of almost immediate equidistribution between the cells, $\lambda \gtrsim 1$, where the two-point statistics barely deviates from the corresponding GOE or GUE prediction (for the figure, we have chosen the case of broken time-reversal invariance where the semiclassical approximation to the random-matrix form factor is exact), to the regime of weak coupling, $\lambda \ll 1$, with $K_0(\tau)$ rising to a marked peak near $\tau = 1$.

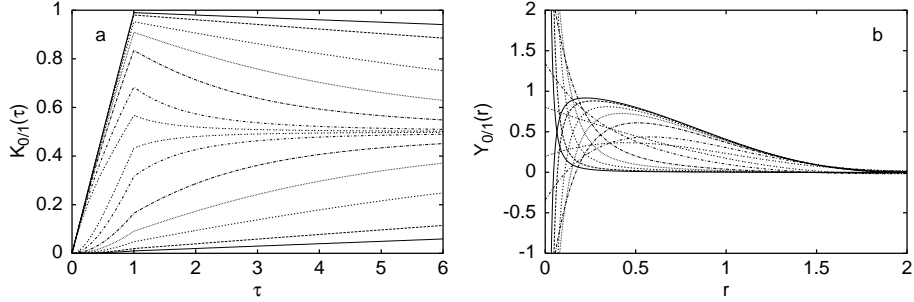


Figure 4. Group-element-specific form factors (a), as described by Eqs. (20) and (46), and corresponding cluster functions (b), for the case of broken time-reversal invariance. In (a), the upper curves show $K_0(\tau)$, the lower curves $K_1(\tau)$. In (b), the graphs with positive initial slope correspond to $Y_0(r)$, those with negative initial slope to $Y_1(r)$. From the outmost to the innermost pair of curves, the decay rate takes the values $\lambda = 0.01, 0.02, 0.05, 0.1, 0.2, 0.5, 1.0$. Graphs of form factors and cluster functions for equal values of λ share a common line signature.

6. Models and numerical results

In the following subsections, we shall introduce four quite diverse types of models that allow to construct systems with two coupled compartments. The numerical results obtained for these models serve to illustrate and check various aspects of the theory developed above.

6.1. The Sinai billiard I

6.1.1. The model and its classical dynamics We construct a two-cell billiard [25] from two parts, each shaped like a quarter of a Sinai billiard [26], and connected by a straight channel between their open sides (Fig. 5). The width of this channel will serve as the basic length unit. The remaining parameters of the billiard are then the length L of the channel and the common radius R of the quarter-circle sections of the boundary.

In the first part of this section, we discuss the central input for the semiclassical theory, the time evolution of $P_{0/1}(t)$, cf. Sect. 2. Since both cells of the billiard support chaotic classical motion, except for bouncing-ball orbits (Fig. 5), we can assume that Eq. (2) holds to a good approximation. We have checked numerically that for the values of R considered, the time for reaching ergodicity in a single cell is indeed negligible against the escape time. We shall describe four alternative methods to determine the escape rate λ .

Consider a single cell of the billiard, detached from the channel, i.e., a quarter Sinai billiard with one of its narrow openings capped. Reflecting it with respect to both straight sections of the outer boundary sections produces a four-disk billiard with

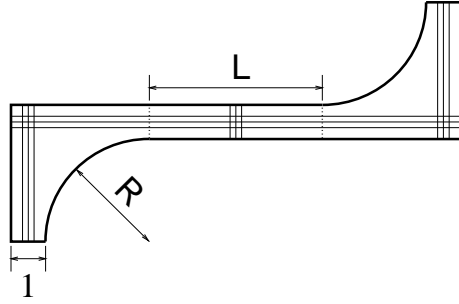


Figure 5. The two-cell Sinai billiard of type I and the three different families of bouncing-ball orbits.

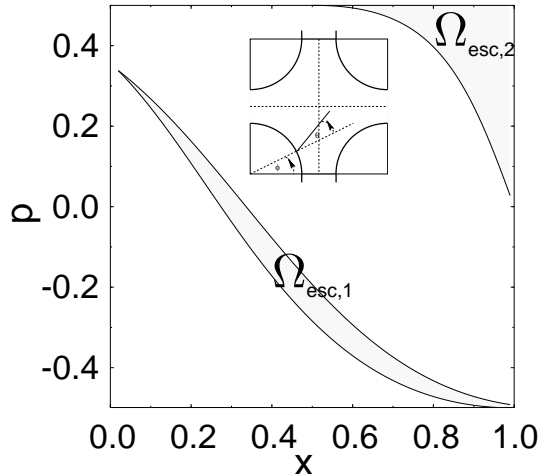


Figure 6. Phase space of the Poincaré map for a single cell of the two-cell Sinai billiard. The parameter value is $R = 5$. Inset: The single cell, extended to a four-disk billiard by reflection with respect to its straight boundary sections (dashed lines), and definition of the basic coordinates ϕ and θ . Dotted and thick lines along the circumference denote open and reflecting sections of the boundary, respectively.

two of its four gaps closed by a reflecting wall, as shown in the inset in Fig. 6. The classical dynamics within the billiard is described by a Poincaré map that connects two successive reflections of a trajectory off the curved parts of the boundary. Employing Birkhoff coordinates, the phase space of this discrete dynamics is spanned by $x = 2\phi/\pi$ and $p = (1/2) \sin \theta$, where ϕ , $0 \leq \phi \leq \pi/2$, and θ , $-\pi/2 \leq \theta \leq \pi/2$, specify site and angle of the reflection, respectively (see the inset in Fig. 6).

The simplest way of finding the rate of escape from the open billiard makes essential use of the assumption that the motion within the billiard is ergodic. The amount of phase-space area leaving the billiard in time dt through a small hole of size s , at unit speed, is then $d\Omega = 2sdt$. By ergodicity, this is to be normalized by the billiard area A

and by 2π , the size of momentum space. The resulting expression for the escape rate is

$$\lambda_{\text{erg}} = \frac{s}{\pi A}. \quad (47)$$

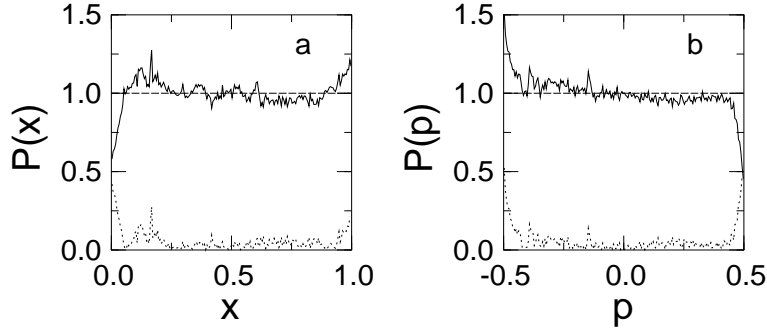


Figure 7. Invariant distributions of the Birkhoff coordinates x (panel a) and p (b) of the Poincaré map for the full two-cell billiard (full lines), and absolute value of their deviation (dashed) from the corresponding constant distribution for the Sinai billiard (horizontal lines).

A similar method determines specifically the relative phase-space measure for leaving the half billiard after one iteration of the Poincaré map,

$$\lambda_{\text{phas}} \approx \frac{\Omega_{\text{esc}}}{\Omega_{\text{tot}}} = \int dx \int dp P(x, p) \chi(x, p). \quad (48)$$

Here, $P(x, p)$ is the normalized invariant phase-space measure for a single cell, and $\chi(x, p)$ is a characteristic function: It equals unity if a trajectory starting at (x, p) leaves with the next iteration, and zero otherwise. In Fig. 7, we compare the invariant distribution for the double billiard, Fig. 5, with that for the closed Sinai billiard. For it, the invariant distribution is constant in x and p . Differences occur close to the extreme values of both x and p . They are due to trajectories leaving one side and returning only after several iterations of the map. In our evaluation of Eq. (48), we have neglected these deviations and set $P(x, p) = 1$.

The escape rate can also be estimated on basis of the unstable periodic orbits of the Poincaré map [27, 28]. It is given by the largest zero of the reciprocal of the dynamical zeta function, considered as a function of time,

$$1/\zeta = \prod_p (1 - t_p). \quad (49)$$

The product in Eq. (49) extends over all periodic orbits of the Poincaré map, and t_p is an amplitude determined by length and stability of the orbit. The evaluation of Eq. (49) is facilitated by applying a cycle expansion and exploiting the symmetries of the system [27, 28].

We have applied this procedure to the fully symmetric four-disk billiard, including only the primitive periodic orbits. The four-disk billiard is different from our actual problem (inset in Fig. 6) in that it has four open sides instead of only two in our case. However, we did not find a way to account, in Eq. (49), for the families of marginally stable bouncing-ball orbits that occur between the two straight boundary sections, and countably infinite sets of unstable periodic orbits that do not fit into the symbol code for the four-disk billiard. Despite these crude approximations, we obtained a reasonable value for λ also by this approach.

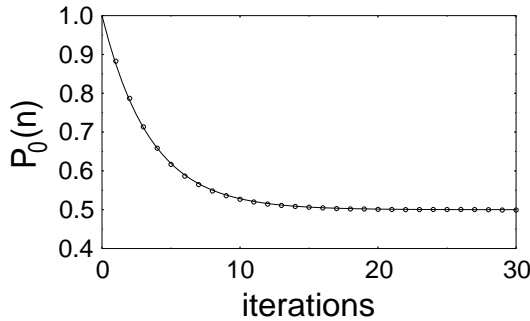


Figure 8. Classical probability to remain in the initial half of the two-cell billiard (dots), compared to an exponential equilibration, Eq. (2) with fitted escape rate (full line), both plotted as functions of the number of iterations of the Poincaré map. The parameter value is $R = 5$.

As a fourth method, we have calculated $P_0(t)$ directly by averaging over 10^6 trajectories, and fitted Eq. (2) to these data (Fig. 8). All values for λ gained within the discrete Poincaré dynamics had to be rescaled to continuous time. To this end, we have determined the distribution of trajectory lengths as a function of the number of iterations of the map and checked that it remains sufficiently narrow to determine a scaling factor. Table 1 summarizes the respective values of the escape rate, obtained for $R = 5$ by the four techniques outlined above.

λ_{erg}	λ_{phas}	λ_{per}	λ_{num}
0.019	0.023	0.021	0.027

Table 1. Escape rates from a half-closed quarter of a Sinai billiard with $R = 5$, determined by the four alternative methods outlined in the text.

6.1.2. Quantization and spectral statistics Quantizing the double billiard amounts to solving the Helmholtz equation

$$\left(\frac{\partial^2}{\partial x^2} + \frac{\partial^2}{\partial y^2} + k^2 \right) \psi(x, y) = 0 \quad (50)$$

with Dirichlet boundary conditions (bc's) on the billiard circumference and a dispersion $k^2 = 2mE/\hbar^2$. Within the connecting waveguide, quantization of transverse momentum, $k_{y,n} = n\pi$, $n = 0, \pm 1, \pm 2, \dots$, implies that there are $N = [k/\pi]$ ([] denoting integer part) open channels with real total momentum $k = (k_x^2 + k_{y,n}^2)^{1/2}$.

The numerical quantization is performed by the scattering-matrix method [23, 17]. It is based on a subdivision of the closed double billiard into two open halves (Fig. 2). Each of them is considered as a chaotic scatterer attached to the end of a semi-infinite waveguide, described by $N \times N$ scattering matrices S^l and S^r , respectively. The secular equation for eigensolutions of the full billiard then reads

$$\det(I - S^l(k)S^r(k)) = 0. \quad (51)$$

In order to construct the $S^{l/r}$ for the billiard halves [23], we start from the $2N \times 2N$ transfer matrix for a quarter Sinai billiard (superscript 's') open on both sides [2, 3],

$$T^s = \begin{pmatrix} rt^{-1}r - t & rt^{-1} \\ t^{-1}r & t^{-1} \end{pmatrix}, \quad (52)$$

Here, t and r denote the $N \times N$ matrices of transmission and reflection amplitudes, respectively. Due to the spatial reflection symmetry with respect to the diagonal, the two entrances of the billiard are equivalent.

The transfer matrix T^w for a waveguide of length $L/2$ consists of phase factors $\exp(\pm i(k^2 - k_{y,n}^2)^{1/2}L/2)$ along the diagonal. The letter-Z-like fashion in which the two halves are assembled is accounted for by a third factor T^z with appropriate phases ± 1 [2, 3] along its diagonal. It is included in the transfer matrix for one of the sides, e.g., $T^l = T^e T^w$, $T^r = T^l T^z$.

The scattering matrices for the billiard halves closed on one side are obtained from T^l and T^r by requiring incoming and outgoing amplitudes to cancel across the openings where Dirichlet bc's are to be enforced,

$$\begin{pmatrix} \mathbf{A} \\ -\mathbf{A} \end{pmatrix} = T^{l/r} \begin{pmatrix} \mathbf{B} \\ \mathbf{C} \end{pmatrix}. \quad (53)$$

Here, \mathbf{A} and $-\mathbf{A}$ refer to the amplitudes at the ends to be closed, and \mathbf{B} and \mathbf{C} to the amplitudes on the opposite sides. The latter are related by $\mathbf{C} = S^{l/r} \mathbf{B}$, invoking the S matrices sought for. Solving for them, one finds

$$S^{l/r} = -(T_{12}^{l/r} + T_{22}^{l/r})^{-1} (T_{11}^{l/r} + T_{21}^{l/r}). \quad (54)$$

In obvious notation, $T_{ij}^{l/r}$, $i, j = 1, 2$, refer to the four $N \times N$ subblocks of the respective transfer matrices. Figure 9 shows a representative example of a pair of eigenfunctions of the double billiard with quasidegenerate eigenenergies.

In order to check the quality of the quantization procedure, we compare, in Fig. 10, the numerical result for the cumulated eigenvalue density with the Brownell formula [29],

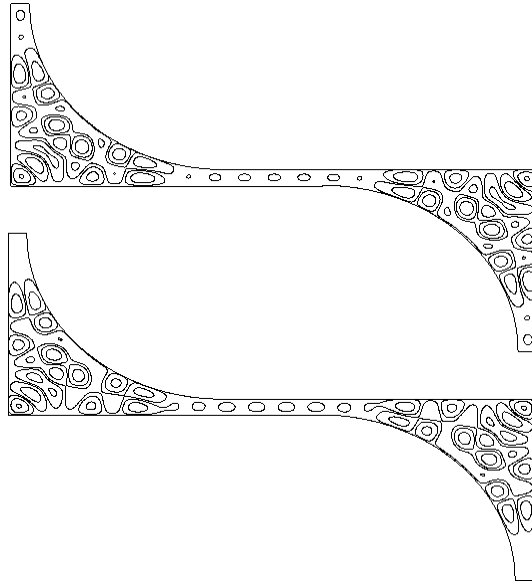


Figure 9. Contour plot of the absolute square of a pair of eigenfunctions of the double billiard with quasidegenerate energies. The state with even symmetry has $k = 3.7569$ (top), the antisymmetric state has $k = 3.7576$ (bottom). The geometric parameter values are $R = 10$ and $L = 5$.

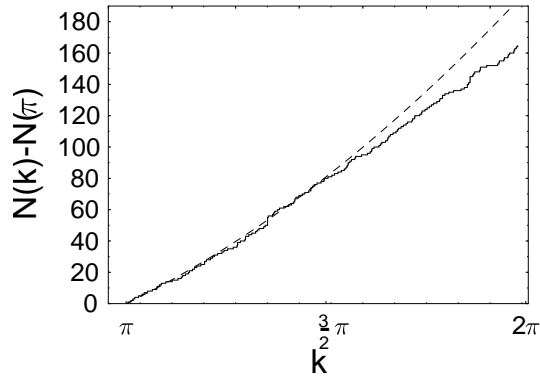


Figure 10. The cumulated eigenvalue density of the double billiard (steps) compared to the Brownell formula (dashed line). The geometric parameter values are $R = 10$ and $L = 10$.

for wavenumbers in the interval $\pi < k < 2\pi$, and $R = 10$. The agreement is satisfactory up to $k \approx 5$. For larger wavenumbers, quasidegenerate pairs of zeros occur in the secular function with too small a spacing to be resolved by the numerical procedure. We have therefore discarded data with $k > 5$. To achieve better statistics in the evaluation of spectral correlations, we have varied L within an interval ΔL amounting to a few percent of L .

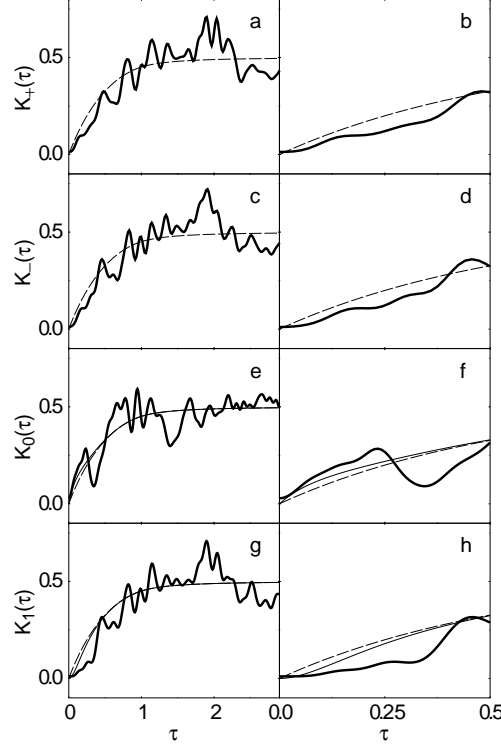


Figure 11. Time evolution of various form factors (heavy lines), compared to a modified semiclassical result (full, see text) and random-matrix theory (broken). The upper two rows show the symmetry-projected form factors (panels a – d), the lower ones the group-element-specific form factors (e – h). The right column consists of blowups of the short-time regime of the data shown on the left. The geometric parameter values are $R = 5$ and $\langle L \rangle = 6.7$.

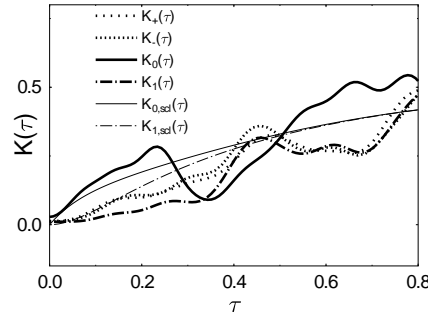


Figure 12. Synopsis of the data shown in Fig. 11.

Figures 11 and 12 are devoted to a comparison of the various form factors, defined in Section 3, with the semiclassical theory. In Fig. 11, we show the symmetry-projected form factors $K_+(\tau)$ (panels a,b) and $K_-(\tau)$ (c,d) (cf. Eq. (11)), as well as the group-element-specific ones $K_0(\tau)$ (panels e,f) and $K_1(\tau)$ (g,h) (cf. Eq. (12)), together with the corresponding predictions of random-matrix and semiclassical theory. In order to achieve a smooth interpolation between the semiclassical result in diagonal approximation and the long-time behaviour of the form factors, we plot, in panels e – h, the functions $K_{\text{GOE}}(\tau)P_{0/1}^{(\text{cl})}(\tau t_{\text{H}})$; see Subsect. 6.2 below. The right-hand column contains blowups of the short-time regime of the data shown on the left. The $K_{\pm}(\tau)$ follow closely the GOE prediction for a single cell of the double billiard, as expected. For short times, $K_0(\tau)$ and $K_1(\tau)$ deviate significantly from the GOE shape, in the way predicted by semiclassical considerations. The initial slope of $K_0(\tau)$ is increased by a factor 2, while that of $K_1(\tau)$ vanishes. In this time regime, there is even quantitative agreement with the semiclassical theory. This is clearly seen in Fig. 12, a synopsis of the four form factors.

For the parameter values underlying the data shown, we have $\lambda t_{\text{H}} \approx 4$, so that classical equilibration between the cells occurs around $\tau \approx 0.125$, cf. Eq. (20). For larger times, the data show strong fluctuations and so are inconclusive anyway. We have checked whether these fluctuations reflect the contribution of bouncing-ball orbits, both in the elbows and in the connecting channel (Fig. 5), with negative result. Our numerical quantization procedure did not allow to go to parameter values where $\lambda t_{\text{H}} \lesssim 0.5$ such that $K_0(\tau)$ is expected to overshoot near $\tau = 1$. The following subsections provide numerical evidence also for this effect.

6.2. The Sinai billiard II

Another example for a two-cell billiard is provided by one half of the Sinai billiard as shown in Fig. 13. A semicircle of radius R divides a rectangle with side lengths L_x, L_y , into two parts connected by an opening of size $s = L_y - R$ along the symmetry axis. The width of this constriction determines the classical rate of transitions between the two cells in the ergodic regime according to Eq. (47). The geometry of this billiard differs from the one discussed in the previous subsection in three respects: The single cells are no longer symmetric in themselves, there is no extra connecting channel of variable length, and the full configuration has reflection rather than inversion symmetry. The main advantage is, however, that there exists a more efficient quantization algorithm [17], again based on the scattering approach [23]. The reflection symmetry allows to compute the eigenvalues in the two parity classes separately by requiring Neumann or Dirichlet bc's along the symmetry axis. We unfold both spectra using the area and circumference contributions to the mean spectral density of one cell [29] and arrive at

the scaled energy eigenvalues.

Our theory, developed in Sections 2 to 5, is based on spectral two-point correlations that indiscriminately include *all* level pairs in the spectrum. The symmetry-based quantization procedure used for the present model, by contrast, gives us immediate access to the scaled eigenvalues $r_{\alpha,\pm}$, presorted according to parity. We take this opportunity to make a few remarks concerning the “genuine” doublets, i.e., level pairs with identical quantum number α but opposite symmetry, and their splittings $r_\alpha = r_{\alpha,-} - r_{\alpha,+}$. We emphasize again that only in the regime of small splittings, statistically independent of the positions of the doublet centers, the two-point statistics embodied in the form factors coincides with the distribution of the genuine doublet splittings, cf. Eq. (26). Outside this regime, the two-point statistics includes separations that are possibly very small but belong to states labeled by different quantum numbers, and therefore do not contribute to the splitting distribution. In effect, the two-point statistics shows more weight at small separations than the splitting distribution.

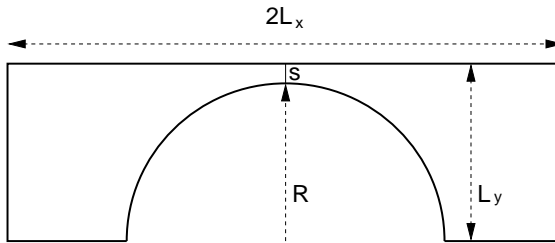


Figure 13. One half of the Sinai billiard consisting of a rectangle and an inscribed circle which divides the system into a reflection-symmetric pair of cells. The numerical data presented in this section correspond to $L_x = 2$, $L_y = 1$, and $s = 0.05$.

Figure 14 shows the individual doublet splittings (dots) and a running average (wiggly line) as a function of the energy. We observe that the average splitting essentially depends on the number $\Lambda = [ks/\pi]$ of open quantum channels in the constriction. For low energy, quasidegenerate doublets prevail. In particular, below the threshold energy of the first quantum channel, we have $0 < |\tilde{r}_\alpha| \ll 1$ for all pairs of eigenvalues. Because of the analogy with actual tunnel splittings [14], we presume that a semiclassical description of the spectrum in this regime should rely on orbits with complex action including the diffractive orbits studied in [30]. This is, however, beyond the scope of the present paper.

As the energy approaches the opening of the first channel, the mean doublet splitting increases exponentially, and doublet splittings larger than the mean level spacing accumulate. Beyond the opening of the second quantum channel, even the average splitting exceeds the mean spacing. Consequently, for high energy, the notion

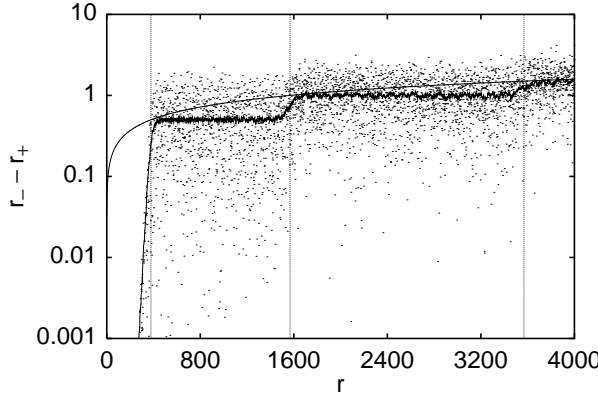


Figure 14. Spacings between pairs of unfolded energy eigenvalues with equal quantum number corresponding to one cell in Fig. 13 and Dirichlet/Neumann boundary conditions along the symmetry axis. The vertical lines mark the threshold energies where the first three quantum channels between the cells open. A running average of the spacings (wiggly line) is compared to the high-energy approximation (smooth curve).

of doublets becomes irrelevant for the spectral statistics of the composite system. It is, though, well suited in the regime of, e.g., a single open quantum channel, as we will show below.

An approximation to the mean value of the doublet spacing is obtained from the asymptotic expansion of the mean spectral staircases \bar{N}_\pm of the two subspectra. While the leading contribution depending on the area A is the same for both spectra, the second term depends on the circumference u and the boundary conditions. For $\hbar = 2m = 1$, we have

$$\bar{N}_-(E) = \frac{A}{4\pi}E - \frac{u}{4\pi}E^{1/2} \quad \bar{N}_+(E) = \bar{N}_-(E) - \frac{s}{2\pi}E^{1/2}. \quad (55)$$

With the approximate quantization condition for scaled energy, $\bar{N}_\pm(E_{\alpha,\pm}) = \alpha + 1/2$ [31], this leads to

$$|r_\alpha| \approx s\sqrt{|r_{\alpha,\pm}|/A\pi}, \quad (56)$$

which is represented by a smooth solid line in Fig. 14. From this figure we see that, for low energy, the approximation (56) is correct only in the vicinity of the channel openings, while the mean splitting is approximately constant between the thresholds. Accordingly, taking the value predicted by Eq. (56) at the opening of the first channel $r = A\pi/4s^2$ for the entire subsequent interval till the next threshold, we find that the mean dimensionless doublet splitting for one open channel is $1/2$ —independently of the size of the hole. Thus it is already of the order of the mean level spacing of the composite two-cell system.

It is an important point that this does not restrict the applicability of our theory: The high probability of large doublet splittings corresponds to the fact that $p_d(r)$ obtained from Eq. (33) has a diverging first moment. Nevertheless, the Fourier transform of it is well-behaved, and beyond the Heisenberg time—where we make use of it—essentially determined by the behaviour of the distribution at small spacings. Indeed, Fig. 14 shows a large number of doublets with a width well below the mean level spacing, which justifies our approach.

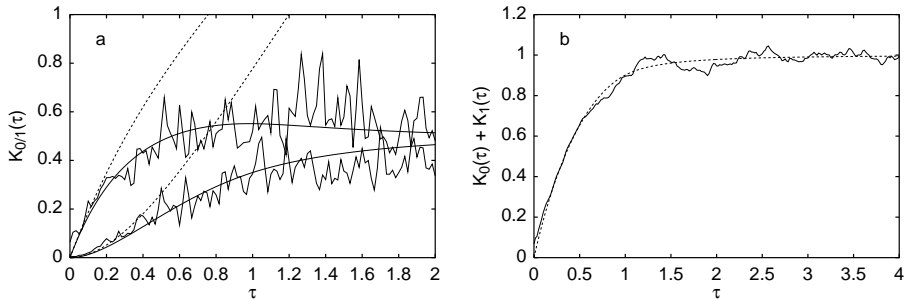


Figure 15. (a) Form factors $K_{0/1}(\tau)$ for the two-cell Sinai billiard of Fig. 13. The dashed lines represent the semiclassical result in diagonal approximation (20), the smooth solid curves correspond to Eq. (57). In (b), $K_0(\tau) + K_1(\tau)$ is compared to the random-matrix result for the form factor of a simple GOE system.

In Fig. 15a, we present the form factors $\tilde{K}_{0/1}(\tau)$ obtained from the 1,187 doublets with one open quantum channel. They were computed after splitting the spectrum into small intervals of 30 doublets each. For the parameter λt_H entering the semiclassical theory we use the value $3/8$ which was obtained assuming ergodicity in analogy to Eq. (47) and inserting for the wave number k the center of the considered interval. The dashed line shows the prediction of the semiclassical diagonal approximation (20), which correctly describes the behaviour of the form factors for small τ , but fails already beyond $\tau \approx 0.2$.

In order to explain this deviation, consider the sum of the group-element-specific form factors $K_0 + K_1$, shown in Fig. 15(b). According to Eq. (13) this is equivalent to the sum of the symmetry-projected form factors, i.e. in the present case the sum of the form factors for Neumann and Dirichlet bc's at the opening. However, the latter represent form factors of two simple GOE systems, which are known to follow the prediction of random-matrix theory, while the diagonal approximation predicts only the correct slope near $\tau = 0$ [16].

To make sure, this fact is demonstrated in Fig. 15b, again using the data from the two-cell Sinai billiard. We conclude that it seems appropriate to combine the correct random-matrix result for a simple GOE system [24] with the semiclassical correction obtained in Section 4 for the symmetric two-cell billiard. Indeed, the resulting expression

$$K_{0/1}(\tau) = K_{\text{GOE}}(\tau) P_{0/1}^{(\text{cl})}(\tau t_{\text{H}}), \quad (57)$$

shown in Fig. 15a with a smooth solid line, provides a satisfactory description of the form factors at least up to the Heisenberg time $\tau = 1$ of one unit cell.

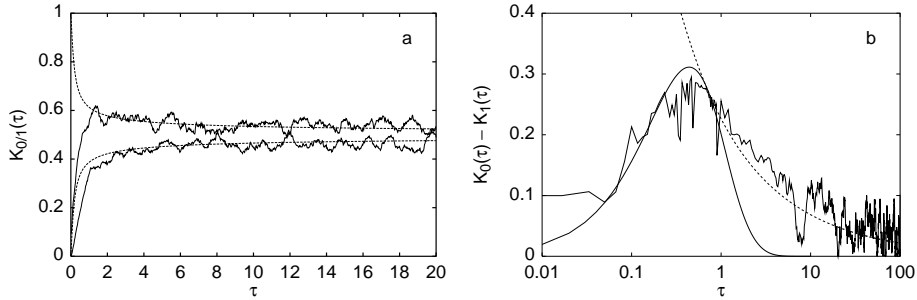


Figure 16. Long-time behaviour of the group-element specific form factors for the two-cell Sinai billiard II. (a) shows $K_{0/1}(\tau)$ together with the prediction according to Eq. (24) (smooth curves). (b) compares the difference of the form factors to the complete theoretical prediction, obtained by matching the semiclassical expression corresponding to Eq. (57) (solid line) smoothly to the long-time behaviour Eq. (35) (dashed line).

In the following, we would like to test the approximation for the long-time behaviour of the form factors. In Fig. 16a, we show how the form factors approach their long-time asymptote $K_0(\tau) = K_1(\tau) = 0.5$, in comparison with the prediction of Eq. (24). The mean resonance width $\langle g \rangle$, which enters our theory via the Fourier transformed doublet-splitting distribution $p_d(\tau)$ Eq. (35), was determined by matching the form factors in the vicinity of the Heisenberg time to the semiclassical result (57). In order to explain this procedure in detail, we show in Fig. 16b, in a semilogarithmic plot, the difference of the group-element-specific form factors, which is beyond $\tau = 1$ equivalent to $p_d(\tau)$, see Eq. (27). For short times, we see again that the quantum data follow reasonably well the random-matrix result corrected by the coarse-grained classical propagator as given in Eq. (57). Unlike the simple diagonal approximation or the case with broken time-reversal invariance, the semiclassical expression (57) allows for a *smooth* transition between the short-time and the long-time approximations: we require that the two curves have a common tangent at some point in the vicinity of $\tau = 1$. This matching has been done numerically, since the involved expressions—though analytically known—are not very transparent. The result $\langle g \rangle \approx 0.25$ obtained in this way, which is in fact not very sensitive to the details of the matching procedure, ensures that our theory describes the long-time behaviour of the form factors over a large time interval with good accuracy and without any free parameter.

6.3. Quantum graphs

In this subsection we construct and investigate a two-cell system consisting of a quantized graph. It was recently shown [18] that quantum graphs exhibit the common quantum signatures of chaos and allow for a formally semiclassical description on the basis of non-deterministic classical dynamics.

A graph is defined by $v = 1, \dots, V$ vertices and $2B$ directed bonds connecting them. The bond b with length L_b is understood to lead from vertex $v(b)$ to $v(\bar{b})$, \bar{b} being the reversed bond ($L_{\bar{b}} = L_b$). On each bond we use a coordinate x_b with $x_b = 0$ at $v(b)$, $x_b = L_b$ at $v(\bar{b})$ and $x_{\bar{b}} = L_b - x_b$. The wave function $\phi_b(x_b)$ satisfies the Schrödinger equation ($\hbar = 2m = 1$)

$$\left(\left[\frac{d}{dx_b} \right]^2 + k^2 \right) \phi_b(x_b) = 0. \quad (58)$$

At the vertices, boundary conditions are chosen such that the current is conserved and the resulting Hamiltonian is self-adjoint and time-reversal invariant. Following the definitions in [18], we require (i), that the wave function is continuous across all vertices, i.e., it has the same value in all bonds b connected to some vertex v

$$\phi_b(0) = \psi_{v=v(b)}, \quad (59)$$

and (ii), that the sum of the momenta in these bonds vanishes

$$\sum_b \delta_{v,v(b)} \frac{d}{dx_b} \phi_b(0) = 0. \quad (60)$$

The eigenvalues of the so-defined graphs can easily be found numerically [18]. For the unit cell, we have interconnected $V = 10$ vertices using $B = 20$ bonds such that each vertex is the intersection of exactly four bonds (inset of Fig. 17b). In this case the classical dynamics is particularly simple: On the bonds, there is free motion at speed $2k$ and each vertex scatters the particle into any attached bond with equal probability $1/4$. On basis of such classical dynamics, a formally semiclassical quantization can be formulated which turns out to be exact in this model.

One of the bonds connecting the two pentagonal layers in Fig. 17b was sectioned, and both ends connected to a second identical unit cell, such that both cells form a ring with translation invariance. The bond lengths L_b of the unit cell are chosen as random numbers, such that the reflection symmetry is broken. The total length is normalized according to $\sum_b L_{b=1}^B = \pi$ and hence the mean level spacing in k of the unit cell is unity. Therefore it is advantageous to use the wavenumber k and the path length L , instead of energy and time, as conjugate variables for the semiclassical description. The Heisenberg time is thus replaced by the Heisenberg length $L_H = 2\pi$ and dimensionless time is introduced as $\tau = L/L_H$. In the ergodic regime, the escape rate from the unit

cell (again with respect to unit path length instead of unit time) is simply given by the inverse total length of the graph, $\lambda = 1/\pi$.

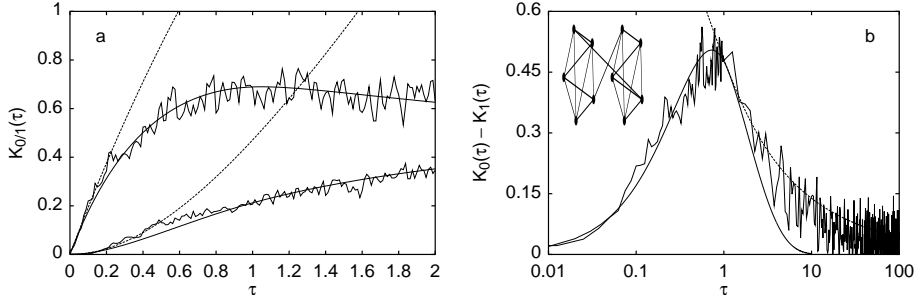


Figure 17. (a) Form factors $K_{0/1}(\tau)$ for the two-cell quantum graph compared to semiclassical expressions as in Fig. 15a. (b) compares the difference of the form factors to the complete theoretical prediction as in Fig. 16b. The inset shows the topology of the unit cell.

It is a particularly nice feature of the model that neither this rate nor the number of quantum channels connecting the two cells depend on energy. Therefore, we can average over arbitrarily large energy intervals. We have computed the form factor from the 10,000 lowest doublets after dividing the spectrum into groups of 40 doublets each. Fig. 17a compares the numerical result to the diagonal approximation (20) and the modified random-matrix result (57). In order to assess the quality of our long-time approximation (35), we choose again a logarithmic representation of $K_0 - K_1$. This quantity contains all interesting information about two-point correlations, since the (complementary) sum $K_0 + K_1$ agrees—as in the case of the Sinai billiard—almost exactly with the random-matrix result (not shown). The parameter $\langle g \rangle$ entering the Fourier transform of the doublet-splitting distribution was again obtained by the smooth matching to the semiclassically corrected random-matrix result described in the previous subsection. Summarizing Fig. 17, we find reasonable agreement of our theory with the numerical data in an interval covering several orders of magnitude in τ .

6.4. The quantum kicked rotor on a torus

The kicked rotor belongs to the class of one-dimensional systems that are rendered classically chaotic only by a periodic driving. Its phase space is spanned by an angle and an angular-momentum variable and therefore has the topology of a cylinder. The nonlinearity of the potential is restricted to its time-dependent component and is controlled by a perturbation parameter. Accordingly, the classical dynamics crosses over smoothly from integrability to global chaos with increasing nonlinearity parameter, thereby following the KAM scenario [32, 33]. The phase space of the kicked rotor

is periodic also with respect to its non-cyclic coordinate, namely along the angular-momentum axis.

Quantum-mechanically, the classical angular-momentum period coexists with \hbar as a second independent action scale. If both are commensurable, then also the quantum kicked rotor is periodic with respect to angular momentum and can serve as a model for solid-state-like systems with discrete spatial translation invariance. Since in the periodic case, the cylindrical phase space may be regarded as being bent back to itself, this variant of the model is referred to as the ‘kicked rotor on a torus’. It is this case which we shall discuss below. If the two angular-momentum periods are incommensurate, the quantum eigenstates are generally localized. In this case, the kicked rotor provides a model for Anderson localization in disordered systems [3, 19]. We will not consider it here.

The kicked rotor is defined by its Hamiltonian

$$H(l, \vartheta; t) = \frac{(l - \Lambda)^2}{2} + V_{\alpha, k}(\vartheta) \sum_{m=-\infty}^{\infty} \delta(t - m\tau). \quad (61)$$

The periodic time dependence implies that spectrum and eigenstates are adequately discussed in terms of quasienergies and Floquet states, respectively. In addition, the kicked rotor may possess two independent antiunitary twofold symmetries, both resembling time-reversal invariance. In order to break them in a controlled manner, an angular-momentum shift Λ has been introduced, and the potential is chosen as [34]

$$V_{\alpha, k}(\vartheta) = k \left[\cos(\alpha \frac{\pi}{2}) \cos \vartheta + \frac{1}{2} \sin(\alpha \frac{\pi}{2}) \sin 2\vartheta \right]. \quad (62)$$

Here, the global prefactor k determines the degree of nonlinearity. The appropriate classical measure of nonlinearity, however, is the parameter $K = k\tau$. If $K \gg 1$, chaotic motion prevails and angular momentum diffuses without restriction by KAM tori.

The ratio of the classical to the quantum period of action is determined by the parameter $\tau/4\pi$. If it is rational, i.e., if $\tau = 4\pi p/q$, with p, q coprime, a unit cell along the angular-momentum axis arises that accommodates q quanta of angular momentum. The number of quasienergy levels per unit cell is then also q . We set $p = 1$ and, in order to avoid an unwanted symmetry of the lattice, require q to be odd.

According to Bloch’s theorem, the spatial periodicity implies the existence of an additional constant of the motion, the Bloch phase θ . It appears explicitly in the symmetry-projected Floquet operator [19],

$$\begin{aligned} \langle l' | \hat{U}(\theta) | l \rangle &= \exp \left(-2\pi i \frac{p}{q} (l - \Lambda)^2 \right) \\ &\times \frac{1}{q} \sum_{n=0}^{q-1} e^{-iV_{\alpha, k}([l+2\pi n]/q)} e^{i(l-l')(l+2\pi n)/q}. \end{aligned} \quad (63)$$

A restriction of the lattice to a finite number of N unit cells, with cyclic boundary conditions at the ends, amounts to discretizing the Brillouin zone so that it comprises N

equidistant values $\theta_m = 2\pi m/N$, $m = 0, \dots, N-1$, of the Bloch phase. The independent parameter N corresponds to the number of levels per band, the total number of levels in the spectrum is Nq .

A system with two unit cells is constructed simply by setting $N = 2$. In contrast to the systems discussed above, the resulting model does not possess a bottleneck between its two compartments, neither in configuration space nor in phase space. A reduced exchange between them therefore comes about solely by slow diffusion. The exchange rate λ is determined by the diffusion constant $D = k^2/2$ (valid if $K \gg 1$) through the simple relation $\lambda = D/(2a^2)$ derived in Appendix A. In the quantum kicked rotor on a torus, the integer q represents the dimensionless size of the unit-cell, to be substituted for a .

The most interesting parameter regime to be studied numerically would be one where $K_0(\tau)$ exhibits the feature indicating quasidegeneracy in the spectrum, a positive peak around $\tau = 1$. For this peak to emerge, the exchange between the cells must be slow. Since there is no bottleneck in the kicked rotor, this can only be achieved through a small diffusion constant. More precisely, it requires that the Heisenberg time should be small against the Thouless time. Measured in units of the discrete time steps of the kicked rotor they are, respectively, $n_H = q$ and $n_D = N^2 q^2 / (\pi D)$, so that the condition for quasidegeneracy to occur reads

$$N^2 \gg \frac{\pi k^2}{2q}. \quad (64)$$

At the same time, it should be avoided that localization becomes effective even within the unit cells, in order to separate the signature of classical diffusion from the direct quantal effect of disorder in the spectrum. The localization length should therefore be kept large compared to the size of the unit cell,

$$\xi \approx \frac{k^2}{4} \gg q. \quad (65)$$

Clearly, both conditions, (64) and (65), can hardly be simultaneously met if N is fixed and small. With $N = 2$, little freedom remains since, in addition, being close to the classical limit and well within the classically chaotic regime requires both q and k to be large. We found that $q = 45$ and $k = 10$ represents an acceptable compromise. The resulting diffusion constant, corrected for oscillations occurring if $K \gtrsim 1$ [32], is $D = 23.23$. We substitute the Thouless time $\tau_D = n_D/q = 2.467$ for the time constant $1/(\lambda t_H)$ of the exponential equilibration.

In Fig. 18, we compare the form factors $K_{0/1}(\tau)$ (panel a) and corresponding cluster functions $Y_{0/1}(r)$ (b) obtained for the quantum kicked rotor on a torus with parameters as above, with our theory, Eqs. (20) and (46). For the evaluation of the theory, we have used the relations cited to determine the decay rate directly from q and k . No fitting was involved. The data cover ten Heisenberg times and thus reach far into the quantum

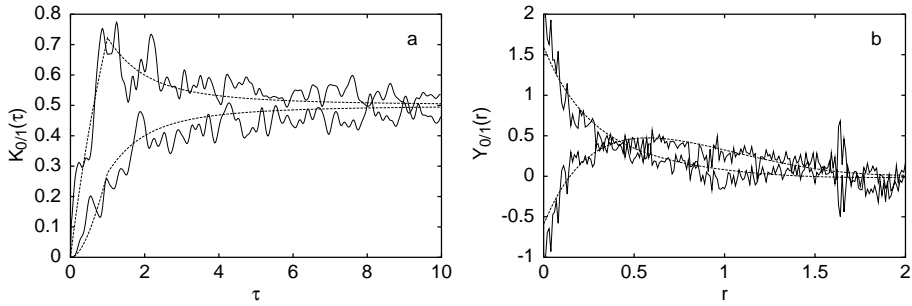


Figure 18. Group-element-specific form factors (a), as described by Eqs. (20) and (46), and corresponding cluster functions (b), for the quantum kicked rotor on a torus, compared with the theory according to Eqs. (20) and (46) (dashed). The parameter values are $q = 45$ and $k = 10$, corresponding to an exchange rate $\lambda = 0.258$.

long-time regime. In the form factors, we can clearly discern the three time domains discussed, the initial phase of chaotic diffusion where $K_0(\tau)$ is strongly enhanced while $K_1(\tau)$ remains close to zero, the sharp positive peak of $K_0(\tau)$, reaching almost twice its asymptotic value, and the saturation regime where $K_0(\tau)$ and $K_1(\tau)$ approach their common asymptote from above and below, respectively. The cluster function for $r \lesssim 1$ represents the regime of long times or small splittings in a different manner. Both plots give evidence that the theory provides a quantitative description of the two-point correlations over all time/energy scales.

7. Conclusion

Chaotic systems with two weakly connected cells, elementary as this concept may appear, form a paradigm for a large class of physical situations and exhibit a surprisingly rich repertoire of behaviour. In this paper, we have shown that it is determined essentially by two parameters. One of them can be identified with the time required for equilibration between the cells, in units of the Heisenberg time of the entire system. It specifies the position between the extreme of a large opening that does not strongly restrict the exchange among the cells, and the opposite extreme of two nearly isolated single cells.

The other relevant parameter is a measure of the difference in shape between the cells, ranging from exact symmetry to its complete absence. The scale on which spatial differences matter is the typical wavelength $2\pi\hbar/\sqrt{2mE}$ of the quantum state.

On basis of the results obtained in this paper, we can draw a clear picture of the spectral two-point correlations in this two-dimensional parameter space. In the case of an effective communication between the cells, the presence or absence of symmetry is of little relevance for the spectral statistics. It is then only the retardation of ergodic

coverage that becomes manifest in the level correlations. It leads to a reduction in the area enclosed by the initial minimum (correlation hole) of the form factor, indicating an increase of randomness in the spectrum which can be completely accounted for by semiclassical considerations [5].

The case of two almost isolated cells lacking all symmetry can be trivially understood from a random-matrix point of view. We are then dealing with the superposition of two spectra that are nearly mutually independent but exhibit the same statistics. Here, random-matrix theory simply predicts a doubling of the time argument of the form factor [22], which is in agreement with the semiclassical approximation in the limit of slow equilibration.

If, in contrast, the two cells are symmetric, the formation of doublets introduces an additional feature to the spectrum. The corresponding positive correlations are reflected in the form factor as a maximum in the vicinity of the Heisenberg time. In the limit of long exchange time, the form factor at this maximum reaches twice the asymptotic value to which it decays subsequently from above, measured from its value at $t = 0$. In the case of exact symmetry, we can quantitatively account both for this peak in the standard form factor and the simultaneous depression in an analogous statistic that refers to transport from one cell to the other, rather than return to the initial one.

The crossover from full to completely broken symmetry, as a function of some symmetry-breaking parameter is still an open issue. Related semiclassical work on spatially periodic systems with slight disorder [35] suggests that the peak in the form factor should decay exponentially with the typical difference in action between symmetry-related periodic orbits in the respective cells. A quantitative theory, however, is still lacking.

Acknowledgments

One of us (TD) would like to thank for the warm hospitality enjoyed during a stay in the group of Prof. O. Bohigas, Institut de Physique Nucléaire, Orsay, where this work was completed. This stay was financed by Deutsche Forschungsgemeinschaft (grant No. Di 511/4-1).

Appendix A. Discrete diffusion

The picture of a two-cell system with the topology of a ring suggests to unroll the ring so that an infinite chain is formed. If the two cells are translation symmetric, then each of them represents a unit cell of this periodic lattice, otherwise the unit cell comprises both cells of the ring. In this extended topology, the condition of slow exchange between the cells implies that the picture of homogeneous diffusion breaks down on the scale of

the lattice constant. We are therefore in a regime opposite to that considered in Ref. [1].

The spreading along the chain is now determined by a master equation for the probability to be at site n , instead of a diffusion equation for the probability density,

$$\dot{P}_n(t) = \lambda P_{n-1}(t) - 2\lambda P_n(t) + \lambda P_{n+1}(t), \quad (\text{A1})$$

In a more concise notation, it reads

$$\left(\frac{d}{dt} - \lambda \Delta_2 \right) \mathbf{P}(t) = 0. \quad (\text{A2})$$

Here, $\mathbf{P}(t)$ denotes the entire infinite vector of the $P_n(t)$, and

$$\Delta_2 = \begin{pmatrix} \cdot & \cdot & \cdot & & & & 0 \\ & \cdot & \cdot & 1 & & & \\ & & 1 & -2 & 1 & & \\ & & & 1 & -2 & 1 & \\ & & & & 1 & -2 & 1 \\ 0 & & & & & 1 & \cdot & \cdot \\ & & & & & & \cdot & \cdot & \cdot \end{pmatrix} \quad (\text{A3})$$

is the discrete Laplace operator. The lattice plane waves

$$\phi_{m,n} = \frac{1}{\sqrt{N}} e^{2\pi i n m / N}, \quad m = 0, \dots, N-1, \quad (\text{A4})$$

where for the sake of normalizability we have reintroduced cyclic boundary conditions with a period of N chain elements, solve the stationary eigenvalue equation

$$\Delta_2 \phi_m = \gamma_m \phi_m \quad (\text{A5})$$

with eigenvalues

$$\gamma_m = 2 \left(\cos \frac{2\pi m}{N} - 1 \right). \quad (\text{A6})$$

For a localized initial state

$$P_n(0) = \delta_{n \bmod N} = \frac{1}{\sqrt{N}} \sum_{m=0}^{N-1} \phi_{m,n}, \quad (\text{A7})$$

the time evolution reads

$$\begin{aligned} P_n(t) &= \frac{1}{\sqrt{N}} \sum_{m=0}^{N-1} \phi_{m,n} e^{\gamma_m t} \\ &= \frac{1}{N} \sum_{m=0}^{N-1} \exp \left(2\pi i \frac{mn}{N} + 2\lambda \left[\cos \frac{2\pi m}{N} - 1 \right] t \right). \end{aligned} \quad (\text{A8})$$

By Poisson resummation, this becomes

$$\begin{aligned} P_n(t) &= \frac{1}{N} \sum_{m=-\infty}^{\infty} \int_0^N d\nu \exp \left(2\pi i \left[m + \frac{n}{N} \right] \nu + 2\lambda \left[\cos \frac{2\pi\nu}{N} - 1 \right] t \right) \\ &= e^{-2\lambda t} \sum_{m=-\infty}^{\infty} I_{|n+mN|}(2\lambda t), \end{aligned} \quad (\text{A9})$$

where $I_n(z)$ denotes the modified Bessel function of integer order n [36]. The spreading over the lattice, as described by $P_n(t)$, represents a discrete diffusion process. If we go to the continuum limit by defining $x = na$, $L = Na$, and letting the lattice constant $a \rightarrow 0$, we recover continuous diffusion with periodic boundary conditions,

$$p(x, t) = \frac{1}{a} P_n(t) \rightarrow \frac{1}{\sqrt{2\pi D t}} \sum_{m=-\infty}^{\infty} \exp \left(-\frac{(x + mL)^2}{2Dt} \right). \quad (\text{A10})$$

The diffusion constant is $D = 2\lambda a^2$. In performing the limit, we have used the asymptotic form of the $I_n(z)$ for large argument z [37] and expanded it for large order n . The two-cell solution, Eq. (2), is retained by setting $N = 2$ in Eq. (A8).

Appendix B. Doublets as discretized bands

As on the level of the classical dynamics, it is instructive to consider also the quantum two-cell system as the unit cell of an infinite chain. From this point of view, the doublets $r_{\alpha,\pm}$ come about by discretizing continuous bands to a “Brillouin zone” with only two points. The simplest possible interpolation assumes cosine-shaped bands,

$$r_{\alpha}(\mu) = R_{\alpha} + r_{\alpha} \cos(\pi\mu), \quad \mu = 0, 1. \quad (\text{B11})$$

Equation (B11) can be justified by the fact that it imposes no more information on the shape of the bands than is available, namely their first two Fourier coefficients. Cosine-shaped bands result also from diagonalizing a two-site, tight-binding Hamiltonian

$$\begin{aligned} H_{n,n'}^{(\alpha)} &= R_{\alpha} \delta_{(n-n') \bmod 2} \\ &+ \frac{1}{2} r_{\alpha} (\delta_{(n-n'-1) \bmod 2} + \delta_{(n-n'+1) \bmod 2}), \\ n, n' &= 0, 1. \end{aligned} \quad (\text{B12})$$

We have defined the parameters of this Hamiltonian in such a way that Eq. (B11) gives its eigenenergies. Inserting them in Eq. (21) and performing a Poisson resummation results in

$$a_n(\tau) = \sum_{m=-\infty}^{\infty} \sum_{\alpha=1}^{N_d} e^{-2\pi i \tau R_{\alpha}} i^{n-2m} J_{2m-n}(2\pi \tau r_{\alpha}), \quad (\text{B13})$$

where $J_k(z)$ denotes the ordinary Bessel function of order k . We introduce a diagonal approximation with respect to the band index α , as in Section 5, and obtain the corresponding form factors as

$$K_n(\tau) = \frac{1}{N_d} \sum_{\alpha=1}^{N_d} \left| \sum_{m=-\infty}^{\infty} (-1)^m J_{2m-n}(2\pi\tau r_{\alpha}) \right|^2. \quad (\text{B14})$$

Invoking the sum rules $\sum_{k=-\infty}^{\infty} (-1)^k J_{2k}(z) = \cos z$, $\sum_{k=-\infty}^{\infty} (-1)^k J_{2k-1}(z) = \sin z$ [38], we recover Eq. (23).

References

- [1] T. Dittrich, B. Mehlig, H. Schanz, and U. Smilansky, *Chaos, Solitons & Fractals* **8**, 1205 (1997); *Phys. Rev. E* **57**, 359 (1998).
- [2] T. Dittrich and U. Smilansky, *Nonlinearity* **4**, 85 (1991); T. Dittrich, E. Doron, and U. Smilansky, *J. Phys. A* **27**, 79 (1994).
- [3] T. Dittrich, *Phys. Rep.* **271**, 267 (1996).
- [4] N. Argaman, Y. Imry, and U. Smilansky, *Phys. Rev. B* **47**, 4440 (1993).
- [5] U. Smilansky, S. Tomsovic, and O. Bohigas, *J. Phys. A* **25**, 3261 (1992).
- [6] N. de Leon and B. J. Berne, *Chem. Phys. Lett.* **93**, 169 (1982).
- [7] M. Brack and R. K. Bhaduri, *Semiclassical Physics*, Frontiers in Physics, vol. 96, Addison Wesley (Reading, Massachusetts, 1987), sect. 8.1 and refs. therein.
- [8] A. Richter et al., preprint, Institut für Kernphysik, TU Darmstadt (1998).
- [9] O. Bohigas, S. Tomsovic, and D. Ullmo, *Phys. Rev. Lett.* **64**, 1479 (1990); **65**, 5 (1990); *Phys. Rep.* **223**, 43 (1993).
- [10] S. Tomsovic and D. Ullmo, *Phys. Rev. E* **50**, 145 (1994).
- [11] R. Utermann, T. Dittrich, and P. Hänggi, *Physica B* **194-196**, 1013 (1994); *Phys. Rev. E* **49**, 273 (1994).
- [12] F. Leyvraz and D. Ullmo, *J. Phys. A* **29**, 2529 (1996).
- [13] P. Leboeuf and A. Mouchet, *Phys. Rev. Lett.* **73**, 1360 (1994).
- [14] S. C. Creagh and N. D. Whelan, *Phys. Rev. Lett.* **77**, 4975 (1996).
- [15] J. H. Hannay and A. M. Ozorio de Almeida, *J. Phys. A* **17**, 3429 (1984).
- [16] M. V. Berry, *Proc. R. Soc. A* **400**, 229 (1985).
- [17] H. Schanz and U. Smilansky, *Chaos, Solitons & Fractals* **5**, 1289 (1995); H. Schanz, *Investigation of Two Quantum Chaotic Systems*, PhD thesis, Logos (Berlin, 1997).
- [18] T. Kottos and U. Smilansky, *Phys. Rev. Lett.* **79**, 4794 (1997).
- [19] F. M. Izrailev, *Phys. Rep.* **196**, 299 (1990).
- [20] M. Tinkham, *Group Theory and Quantum Mechanics*, MacGraw-Hill (New York, 1964).
- [21] J. M. Robbins, *Phys. Rev. A* **44**, 2128 (1989).
- [22] O. Bohigas, in *Chaos and Quantum Physics*, Les Houches Lectures LII, M.-J. Giannoni, A. Voros, and J. Zinn-Justin (eds.), North-Holland – Elsevier (Amsterdam, 1992), p. 87.
- [23] E. Doron, U. Smilansky, and A. Frenkel, *Physica D* **50**, 367 (1991); E. Doron and U. Smilansky, *Nonlinearity* **5**, 1055 (1992).
- [24] T. A. Brody, J. Flores, J. B. French, P. A. Mello, A. Pandey, and S. S. M. Wong, *Rev. Mod. Phys.* **53**, 385 (1981).

- [25] G. Koboldt, Diploma thesis, University of Augsburg, unpublished (1997).
- [26] Y. G. Sinai, Sov. Math. Dokl. **4**, 1818 (1963).
- [27] P. Cvitanović and B. Eckardt, Phys. Rev. Lett. **63**, 823 (1989).
- [28] P. Cvitanović, Nonlinearity **6**, 277 (1993).
- [29] H. P. Baltes and E. R. Hilf, *Spectra of Finite Systems*, Bibliographisches Institut (Zürich, 1976).
- [30] H. Primack, H. Schanz, U. Smilansky, and I. Ussishkin, Phys. Rev. Lett. **76**, 1615 (1996); J. Phys. A **30**, 6693 (1997).
- [31] R. Aurich, C. Matthies, M. Sieber, and F. Steiner, Phys. Rev. Lett. **68**, 1629 (1992).
- [32] A. J. Lichtenberg and M. A. Lieberman, *Regular and Stochastic Motion*, Applied Mathematical Sciences, vol. 38, Springer (New York, 1983).
- [33] B. V. Chirikov, Phys. Rep. **52**, 263 (1979).
- [34] R. Blümel and U. Smilansky, Phys. Rev. Lett. **69**, 217 (1992); M. Thaha, R. Blümel, and U. Smilansky, Phys. Rev. E **48**, 1764 (1993).
- [35] T. Dittrich, B. Mehlig, H. Schanz, and U. Smilansky, to be published.
- [36] M. Abramowitz and I. A. Stegun, *Pocketbook of Mathematical Functions*, Harri Deutsch (Thun, 1984), p. 118.
- [37] *idem*, p. 121.
- [38] *idem*, p. 187.